Journal of Applied Polymer Science

Efficiency of silver-based antibacterial additives and its influence in thermoplastic elastomers

Daiane Tomacheski,[1,2] Michele Pittol,[2] Vanda Ferreira Ribeiro,[1,2] Ruth Marlene Campomanes Santana[1]

[1]Department of Materials Engineering, Laboratory of Polymers – LAPOL, Federal University of Rio Grande do Sul, UFRGS, 9500 Bento Gonçalves Avenue, Postal Code 15010, Porto Alegre 91501-970, Brazil

[2]Softer Brasil Compostos Termoplásticos LTDA, 275 Edgar Hoffmeister Avenue, Campo Bom 93.700-000, Brazil

Correspondence to: D. Tomacheski (E-mail: daitomacheski@gmail.com)

ABSTRACT: Styrene-butylene/ethylene-styrene-based thermoplastic elastomers (TPE) are polymers with soft touch properties that are widely used for manufacturing devices that involve hand contact. However, when contaminated with microorganisms these products can contribute to spreading diseases. The incorporation of antibacterial additives can help maintain low bacteria counts. This work evaluated the antibacterial action of TPE loaded with silver ions and silver nanoparticles. The additives nanosilver on fumed silica (NpAg_silica), silver phosphate glass (Ag^+_phosphate), and bentonite organomodified with silver (Ag^+_bentonite) were added to the TPE formulation. The compounds were evaluated for tensile and thermal properties and antimicrobial activity against *Escherichia coli* (*E. coli*) and *Staphylococcus aureus* (*S. aureus*). All the additives eliminated over 90% of *E. coli*, but only NpAg_silica killed more than 80% of *S. aureus* population. The better effect of NpAg_silica was attributed to the additive's high specific surface area, which promoted greater contact with bacteria cells. © 2016 Wiley Periodicals, Inc. J. Appl. Polym. Sci. **2016**, *133*, 43956.

KEYWORDS: elastomers; nanoparticles; nanowires and nanocrystals; properties and characterization; thermoplastics

Received 26 January 2016; accepted 22 May 2016

DOI: 10.1002/app.43956

INTRODUCTION

Styrene-ethylene/butylene-styrene (SEBS)-based thermoplastic elastomers (TPE) are polymers with soft touch properties that are widely used for manufacturing medical and personal devices that involve hand contact such as toothbrush cables, cell phones, keyboards, wheelchair handlebars, and pens.[1] These objects are susceptible to biofilm formation, contributing to spreading diseases, mainly in hospital environments, where infections can be transmitted through health care worker's hand.[2] Moreover, the microbial attack causes damage to the mechanical properties, surface degradation and staining, resulting in a deteriorated appearance.[3,4] Microbial adherence to a polymeric surface is a requirement for biofilm formation.[5] On this basis, the development and use of polymers with an antibacterial feature, together with disinfection protocols, can prevent the dissemination of pathogens in several environments.[6,7]

Despite numerous studies about silver in polymeric matrices such as polypropylene,[8,9] polyethylene,[10,11] polyamide,[12] polyethylene terephthalate and polyvinyl chloride,[13] polystyrene,[14] and even thermoplastic polyurethane,[15] to our knowledge, no studies have been conducted regarding antibacterial properties of silver in SEBS-based TPE.

Antibacterial materials containing a set of organic and inorganic substances have been developed.[16,17] Inorganic biocides have attracted much interest for bacterial control due their heat resistance, durability, and selectivity toward microorganisms.[18,19] In the case of silver (Ag)-based materials, the low volatility, broad microbial spectrum killing, and rare cases of bacterial resistance are relevant characteristics for its choice as an antibacterial agent.[20] Moreover, efforts have been made aiming to improve its biocide efficiency.

It is well known that bioavailability of silver species will impact on metal antibacterial characteristics.[21] Elements such as particle size,[15] surface specific area,[12] and precursor materials[21] of particles may contribute to metal availability and bactericidal performance of polymer incorporated with silver. It is assumed that to obtain an antibacterial effect, silver ions must be released from the bulk to the aqueous medium, in this way, further on silver elemental form, a range of silver modifications have been tried, such as carbon nanotubes with silver,[22] silver/silica nanocomposites,[23] colloidal silver,[24] zeolites doped with silver,[25] silver nanoparticles,[26] and silver nanocomposites with bacterial and cellulosic fibers.[27] Also, the processes in which silver particles are incorporated into the polymeric matrix (blending,

© 2016 Wiley Periodicals, Inc.

embedding or coating) can influence the biocide action by affecting the molecular contact between the silver and the polymer surface.[28–30] Ag-based TPE systems must be capable of being manufactured by model processing, and the product should be extruded and injection molded, while keeping proper antibacterial agent concentration. In addition, depending on the type of application, the materials have to possess certain mechanical, rheological, thermal and chemical resistance, and stability under harsh processing situations.[8] Particles with Ag can be incorporated into TPE during the extrusion process by melt blending, which is the most usual method to provide biocide properties to polymers.[31]

Understanding the mechanisms of action between the type of silver used and their mechanical performance and antibacterial efficiency will lead to proper selection of an agent for manufacturing antibacterial TPE products. In the present study, the TPE/silver compounds were prepared via extrusion process, with the aim of to evaluate the effects of nanosilver adsorbed on fumed silica (NpAg_silica), silver ions supported in phosphate glass (Ag^+_phosphate), and bentonite organomodified with silver (Ag^+_bentonite) on the mechanical and antibacterial properties of thermoplastic materials.

EXPERIMENTAL

Materials

The additives tested were nanosilver adsorbed on fumed silica (NpAg_925-SiO, supplied by TNS Nanotecnologia Ltda. and named here as "NpAg_silica") silver ions supported in phosphate glass (named here as "Ag^+_phosphate") and bentonite organomodified with silver (Bactiblock 101 R1.43, supplied by Nanobiomatters BactiBlock, S.L. and named here "Ag^+_bentonite") as biocide. The proportions used were those recommended by the additive suppliers; 0.025–0.05, 0.1–0.3%, and 0.5–2.0%, respectively. The additives were added to a TPE formulation compounded by styrene-ethylene/butylene-styrene copolymer (SEBS, 32% styrene, ethylene/butylene 32/68, linear, M_w 214.8 g mol^{-1}, $M_w/M_n = 1.3$), polypropylene homopolymer (PP, melt flow index 1.5 g 10 min^{-1} at 230 °C), white mineral oil (64% paraffinic and 36% naphtenic), in the ratio of 30/20/50, respectively. Antioxidant Irganox 1010 (0.1%) was added to avoid thermal degradation during processing. A standard sample (additive free) was also used.

Compound Preparation

The samples were prepared using a co-rotating double screw extruder (L/D 40 and 16 mm screw diameter, AX Plásticos) with temperature profile from 170 to 190 °C, speed screw of 300 rpm, feed rate of 1.5 kg h^{-1} and melt discharge temperature of 200 °C. The extrusion parameters were kept constant throughout the tests. Specimen in plate form of 2 mm thick were prepared using injection molding machine (Haitian, PL860) at 190 °C and an injection pressure of 17 bars. After molding, the specimens were conditioned at 23 ± 2 °C and 50 ± 5% relative humidity for 24 h before testing.

Compounds and Additives Characterization

Additive's Mineral Compositions. The additive's mineral compositions were determined by qualitative analysis by X-ray diffraction in Pan Analytical X'pert PRO and X'Pert HighScore software.

Particle Size Measurement. Particle size distribution was determined by laser diffraction in a CILAS 1180 particle size analyzer with scanning range from 0.04 to 2500 μm. NpAg_silica and Ag^+_phosphate were predispersed in deionized water using ultrasound (60 s) and Ag^+_bentonite was predispersed in isopropyl alcohol.

Particles Specific Surface Area (SSA). The SSA of particles was measured by nitrogen adsorption using the Brunauer–Emmett–Teller (BET) method. Measurements were performed by a Quantachrome Nova 1000e surface area analyzer. Samples were dried in an oven at 110 °C for 24 h and then in vacuum at 200 °C for 3 h.

Analysis of Fourier Transform Infrared Spectroscopy Spectra. Fourier transformed infrared spectroscopy attenuated total reflection (FTIR–ATR) was recorded on a PerkinElmer spectroscope (Frontier). Each spectrum was recorded with a total of 10 scans; at a resolution of 4 cm^{-1} at room temperature. The Spectrum software was used for spectra analysis.

Scanning Electron Microscopy Analysis. Morphological analysis of the samples was performed with scanning electron microscopy (SEM), where the samples were deposited in carbon type stuck to stub, metalized with gold, compounds were cryogenically broken in liquid nitrogen. For image acquisition, a SEM of field emission (SEM-FEG) (Inspect F50, FEI) was used with 20 kV, spot 3, and working distance of 10 mm.

Transmission Electron Microscopy Analysis. For transmission electron microscopy (TEM) (Tecnai, G2 T20), additives were dispersed in ethanol by ultrasound for 30 minutes. The samples were prepared by placing a drop of the ethanol suspension onto a small carbon film coated copper grid (300 mesh). For compounds images, ultrathin sections (70 nm) were prepared with a Leica EM FC7 ultramicrotome with a diamond knife. For image acquisition an acceleration voltage of 200 kV was used. The average particle diameter was calculated using ImageJ version 1.40g software.

Mechanical Properties. The mechanical properties of the compounds were obtained by tensile test and analyzed according to ASTM D 412C, in the EMIC DL 2000 machine. The cross-head speed and gauge length of the apparatus were 500 mm min^{-1} and 25 mm, respectively.

Differential Scanning Calorimetry. Thermal analysis of the samples by differential scanning calorimetry (DSC) was performed in a DSC Q100 (TA Instruments). The samples were subjected to heating from −30 °C to 200 °C at a heating rate of 10 °C min^{-1}. The desired temperature was maintained for 5 min and cooled to −30 °C at the same rate, and reheated under a nitrogen atmosphere. Crystallinity values were obtained in the heating second cycle. Nitrogen was used at a flow rate of 50 mL min^{-1}. The degree of crystallinity X_c, normalized to crystalline phase of compositions, PP, as suggested by Karakaya (2010)[32] by applying the eq. (1):

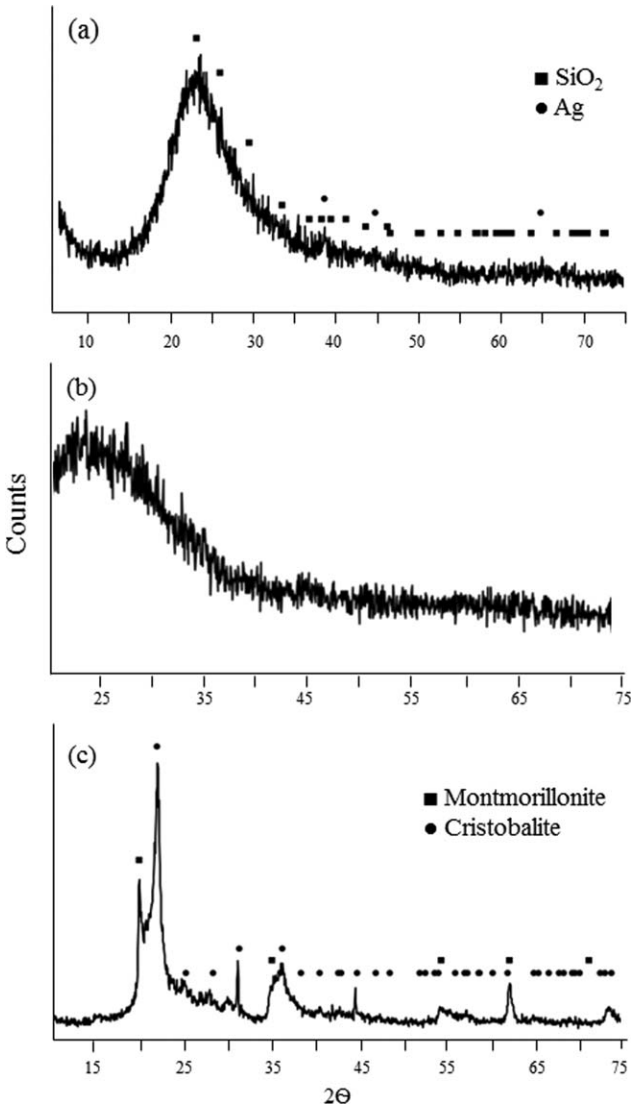

Figure 1. Diffractograms of samples: (a) NpAg_silica, (b) Ag^+_phosphate, and (c) Ag^+_bentonite.

$$X_c(\mathrm{PP}) = \frac{\Delta H^*(\mathrm{PP})}{w \times \Delta H^0 PP} \times 100 \quad (1)$$

where ΔH is the enthalpy of fusion per gram, w is the PP fraction found in the compound, and ΔH^0(PP) is the enthalpy of fusion per gram of 100% crystalline PP (209 J g^{-1}).[33]

Antimicrobial Studies. Japan industrial standard (JIS) Z 2801:2010[34] was applied to evaluate antibacterial efficiency of samples against *Staphylococcus aureus* ATCC 6538 (*S. aureus*) and *Escherichia coli* ATCC 8739 (*E. coli*) strains. TPE specimens (50 mm × 50 mm) were placed in a sterile Petri dish and 400μL of 6×10^6 CFU cm^{-2} of *E. coli* and 3×10^6 CFU cm^{-2} of *S. aureus* suspension were inoculated on the specimen surface. All of them were incubated for 24 h at 35 ± 1 °C. The result was expressed as a microbial value calculated from the difference between the number of colony forming units (CFU) per square centimeter at zero hour (initial) and after 24 h of incubation, eq. (2):

$$E_f(\%) = \frac{P_i - P_f}{P_i} \quad (2)$$

where E_f is the reduction of bacterial population (percentage, %), P_i and P_f are, respectively, initial and final bacterial population (CFU per square centimeter, CFU cm^{-2}).

Antibacterial activity – R, was validated in accordance with JIS Z 2801, with the eq. (3):

$$R = U_t - A_t \quad (3)$$

Where U_t is average of logarithm numbers of viable bacteria after inoculation on standard (additive free) samples after 24 h and A_t is average logarithm numbers of viable bacteria after inoculation on antibacterial samples after 24 h. To be considered effective, R must be ≥ 2.0.

Statistical Analysis. Statistical analysis of variance was applied in tensile strength, modulus, elongation at break and antibacterial results using MYSTAT, student version 12 (Systat Software, Inc., CA). The level of significance was set at 0.05.

RESULTS AND DISCUSSION

Additive Characterization

Additive's Mineral Compositions. X-ray diffraction detected the presence of SiO_2 (JCPDS 01-082-1557) and Ag (JCPDS 01-087-0720) in the NpAg_silica sample [Figure 1(a)]. The Ag^+_phosphate sample has an amorphous structure, so it was not possible to characterize its composition through this method [Figure 1(b)]. The Ag^+_bentonite sample contain montmorillonite-22A (JCPDS 00-029-1499) and cristobalite (JCPDS 01-077-1317) [Figure 1(c)].

Particles Specific Surface Area. The specific surface area (SSA) of the additives is shown in Table I. NpAg_silica showed the highest SSA, 293.9 m^2 g^{-1}, as expected for nanoparticles.[23] Ag^+_phosphate have the lowest SSA, 6.16 m^2 g^{-1}. The SSA found in Ag^+_bentonite, 36.73 m^2 g^{-1}, is in accordance with the literature inspection.[35,36]

Morphological Analysis. Figure 2 shows images obtained by SEM (left) and TEM (right). Figure 2(a,b) show micrographs of NpAg_silica sample obtained in SEM and TEM, respectively. In SEM images, it was possible to observe blocks with irregular geometry and the same size determined before in laser diffraction (between 5 and 30 μm). The TEM images confirmed nanoscale of this additive, with nanoparticles of silica (20 nm) and silver (10 nm), both in spherical forms. In this study, as reported previously by Egger *et al.* (2009)[23] in SEM image of NpAg_silica were observed the silver nanoparticles located on the surface of the silica matrix and also embedded in a matrix of amorphous silicon dioxide (SiO_2). This shape provides a quick availability of silver to the compound.

Table I. Specific Surface Area Determined by BET

	NpAg_silica	Ag^+_phosphate	Ag^+_bentonite
SSA (m^2 g^{-1})	293.90	6.16	36.73

BET: Brunauer–Emmett–Teller method.

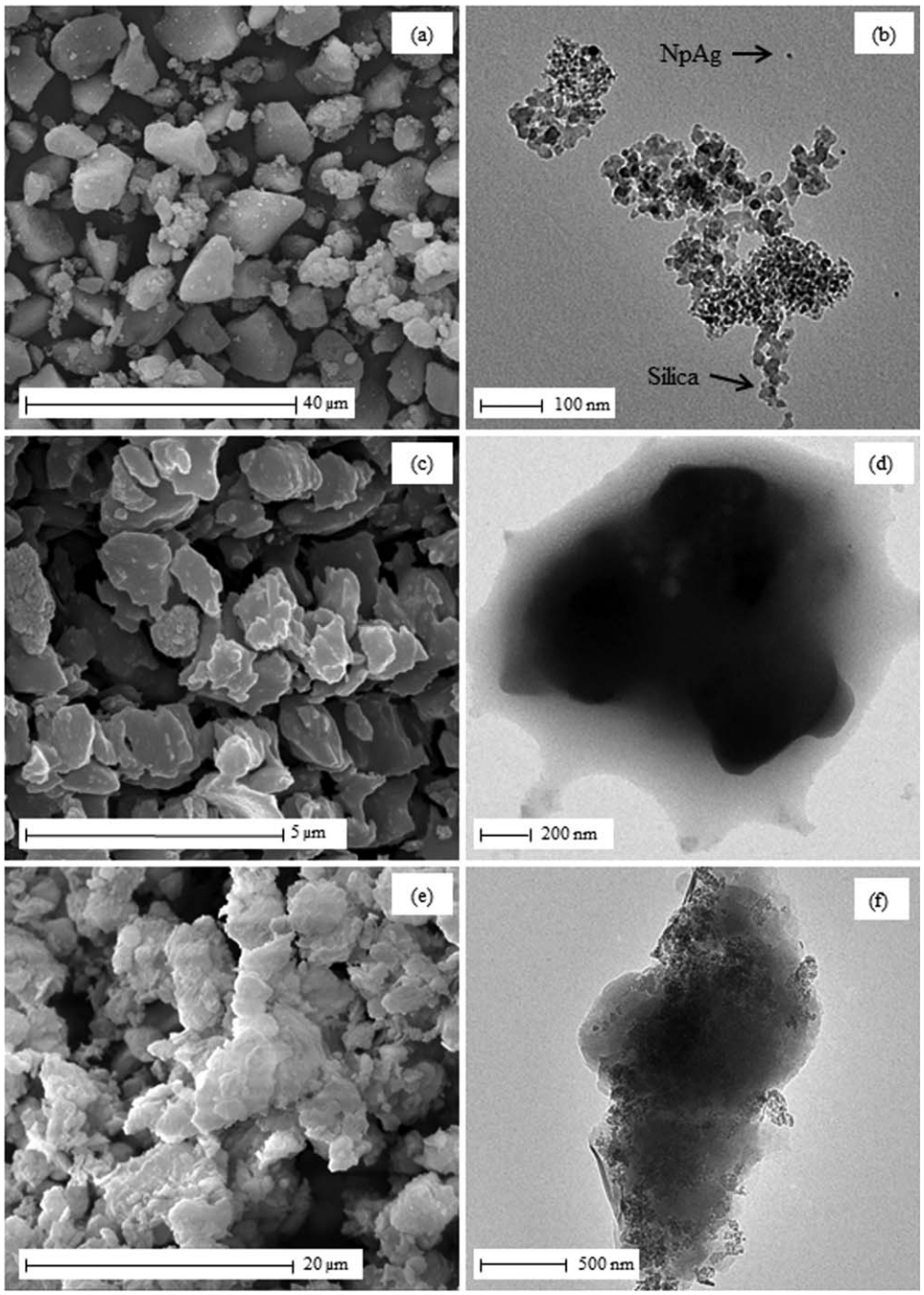

Figure 2. Micrographs of SEM (left) and TEM (right) of additives: (a,b) NpAg_silica, (c,d) Ag^+_phosphate, and (e,f) Ag^+_bentonite.

As seen on Figure 2(c,d), Ag^+_phosphate presented a non-crystalline planar form. In a study performed by Suenaga *et al.* (2003),[37] the authors found that the silver ions present a tetrahedral molecular configuration and create a two-dimensional sheet composition including dimeric units. In SEM image, the particles presented 2 µm, the same size determined by granulometric assay. The results obtained in granulometric and SEM assay reflect the agglomerate patterns of the Ag^+_phosphate particles. In TEM images, the particles presented 200 nm in size.

Ag^+_bentonite [Figure 2(e,f)] showed a typical platelet form found in montmorillonite clay.[38] In this sample, difference in size was observed between the SEM and granulometric results. In SEM and granulometric assay, particles presented an average size of 10 µm, while in TEM their size was 1 µm. The difference in size can be attributed to the agglomerated sheets configuration which prevents measurements. It was not possible to identify traces of silver in the micrographs of additives Ag^+_phosphate and Ag^+_bentonite.

Particle Size Measurement. Values of average diameter, D_{10}, D_{50}, and D_{90} determined by laser diffraction are shown in Table II. It was noted that the average size of the NpAg_silica (12.97 µm) showed a value above the nanoscale. This result reflects the

Table II. Values of Average Diameter, D_{10}, D_{50}, and D_{90} Determined by Laser Diffraction

	Average diameter (μm)	D_{10} (μm)	D_{50} (μm)	D_{90} (μm)
NpAg_silica	12.97	4.7	9.2	28.99
Ag^+_phosphate	1.61	0.86	1.50	2.49
Ag^+_bentonite	7.30	2.08	6.32	13.92

size of the NpAg_silica clusters, as observed in TEM and SEM images shown above. Ag^+_phosphate have an average size of 1.6 μm. Ag^+_bentonite has an average size of 7.30 μm, ranging from 2.08 to 13.92 μm.

Analysis of Fourier Transform Infrared Spectroscopy Spectra. Figure 3 shows the infrared spectra of NpAg_silica, Ag^+_phosphate, and Ag^+_bentonite, in the region ranging from 1600 to 650 cm^{-1}.

In the NpAg_silica spectra [Figure 3(a)], a peak on 1070 cm^{-1} was observed and attributed to Si–O–Si asymmetric stretching.[41] An ideal stoichiometric silicon dioxide is 1080 cm^{-1}. The Si-O stretching peaks are at 792 cm^{-1}. In silicon dioxide infrared, there was a dependence of the peak position and the oxygen

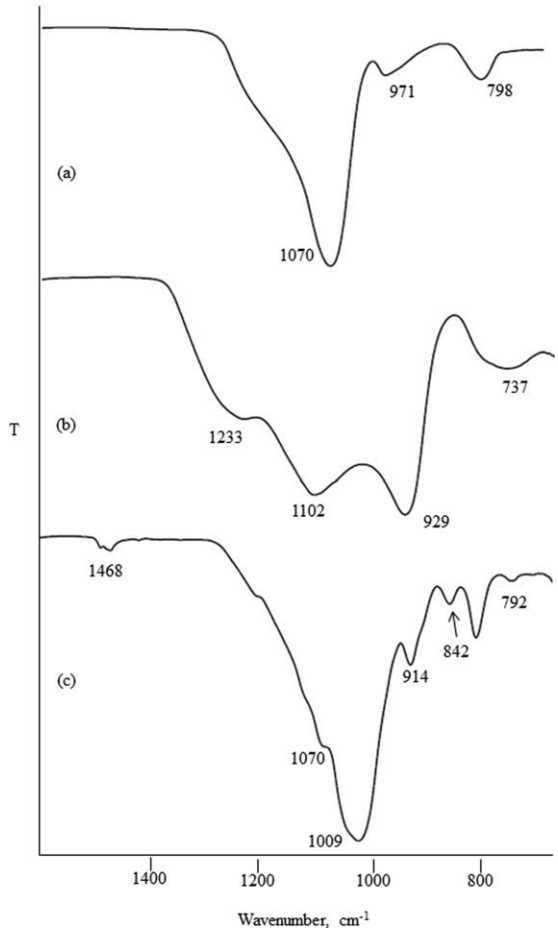

Figure 3. FTIR-ATR spectra of (a) NpAg_silica, (b) Ag^+_phosphate, and (c) Ag^+_bentonite.

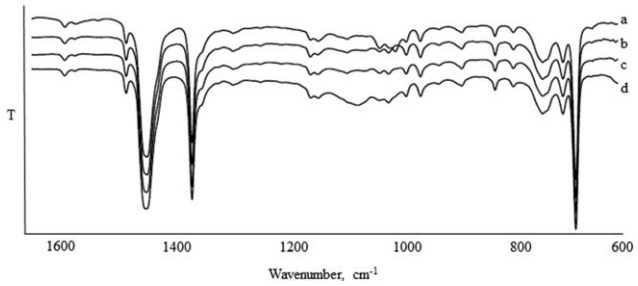

Figure 4. FTIR-ATR spectra of the (a) standard sample and compounds with (b) 0.05% of NpAg_silica, (c) 0.3% of Ag^+_phosphate, and (d) 2% of Ag^+_bentonite.

dose, ranging from 1015 to 1080 cm^{-1}, the higher the oxygen amount the greater will be the peak position (SiO_x, with $x \approx 2$).[39,40] Also, the absorption of around 800 and 960 cm^{-1} is related to the rocking, bending and stretching vibrational modes of the Si–O–Si units, respectively.[40,41]

In Figure 3(b), symmetric stretching of P—O—P in P_2O_7 can be seen at 737 cm^{-1}, symmetric stretching of P-O in PO_3 and PO_4, and asymmetric stretching of P—O—P in P_2O_7 can be seen at 929 cm^{-1}. Asymmetric stretching of P-O in PO_3 and PO_4 can be seen at 1102 and 1233 cm^{-1}. As observed in the Ag^+_phosphate FTIR analysis, phosphate peak can be superimposed by other peaks.[42,43]

Figure 3(c) shows the infrared of Ag^+_bentonite, the peaks in 1009 and 1070 can be attributed to Si—O—Si bonds[39–42]; peaks 842 and 914 cm^{-1} are attributed to deformations in (MgAlOH) and (AlAlOH).[35–44] Silicon and oxygen are common to all clay minerals. Their combination with other elements, such as aluminum, magnesium, iron, sodium, calcium, and potassium, and the ways in which these elements can be linked provide a large number of configurations.[38]

Compound Characterization

Analysis of fourier transform infrared spectroscopy spectra. Infrared spectra from standard and additived compounds with 0.05% of NpAg_silica, 0.03% of Ag^+_phosphate and 2.0% of Ag^+_bentonite were analyzed to evaluate possible modifications in molecular organization due to the incorporation of additives. There were not changes in the region 1200–600 cm^{-1} as show on Figure 4. It was possible to notice the characteristics bands of SEBS in 699 and 759 cm^{-1} due to out-of-plan bending of C-H in aromatic monosubstituted ring of styrene units.[45] Skeletal vibrations representing C=C stretching of aromatic styrene ring appeared at 1493 cm^{-1} [45] and rocking vibration of CH_2 from ethylene appear at 720 cm^{-1}.[46] Bands in 1452 and 1376 cm^{-1} were in plane bending of the C-H from CH_2 and CH_3, common to all components of the blend.[45,46]

Tensile Properties. Figure 5 shows the results of tensile properties of the compounds. There were not significant changes in tensile strength and elongation at break values of specimens with biocide when compared to the standard specimen. However, the modulus values presented a significant difference when compared with loaded compounds ($P < 0.05$), but it cannot be related to a particular additive. Modulus can be affected by

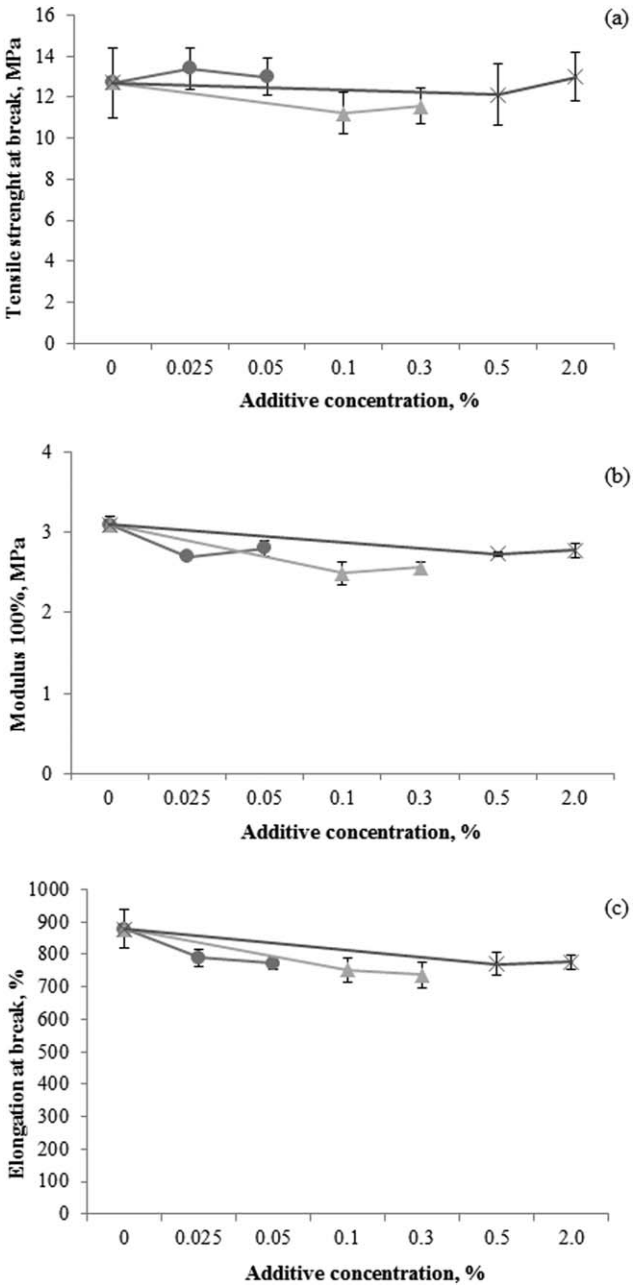

Figure 5. Variation in tensile properties of the compounds: (-•-) NpAg_-silica, (-▲-) Ag^+_phosphate and (-x-) Ag^+_bentonite. Note: ANNOVA test: Tensile strength ($F_{6,28} = 2.223$; $P = 0.07$), modulus ($F_{6,28} = 25.461$; $P < 0.05$) and elongation at break ($F_{6,28} = 2.124$; $P = 0.08$).

moduli of the two phases, as well as volume fraction, particle geometry, degree of agglomeration, and size distribution of particles (Xanthos, 2010).

Wu *et al.* (2005)[47] found that surface characteristics of particles are very important to improve dispersion and interface between particle and matrix. Also, high interfacial stiffness improves polymer modulus. If particle and matrix are not properly matched, the contact point between both surfaces will be a weak point that will reduce the modulus.[48,49] Based on this information, it could be concluded that there was no interfacial adhesion between the additives and polymer.

Differential Scanning Calorimetry. In Figure 6 are shown overlapping curves of exothermic and endothermic events corresponding to the crystallization and melting of polypropylene. It was observed a slight shift to the right of the crystallization temperature in loaded samples compared to sample standard (additive free, curve a). Regarding to the endothermic curves, there was no significant difference in the melting temperatures between standard sample and loaded samples.

Table III shows the values of melting temperature (T_m), fusion enthalpy (ΔH_m), crystallization temperature (T_c), crystallization enthalpy (ΔH_c), and crystallinity degree (X_c) of the compounds.

The crystallization temperature of pure PP used in this work was 113 °C, in the form of the compound it was decreased to 107 °C, and with the incorporation of additives changed to 108 °C. As shown in Table III, all the samples had a T_m around 153 °C, lower than melt temperature of pure PP that was 166 °C. This result confirms that the addition of SEBS and oil into PP restricts the mobility and packing of PP chains. In a study realized by Karakaya *et al.* (2010),[32] the addition of filler increases the crystallinity degree and was attributed to action of the particles as nucleating agents. In general, there was a slight increase in X_c values with the additives incorporation, but this values were similar to standard sample, and therefore, may be considered not significant.

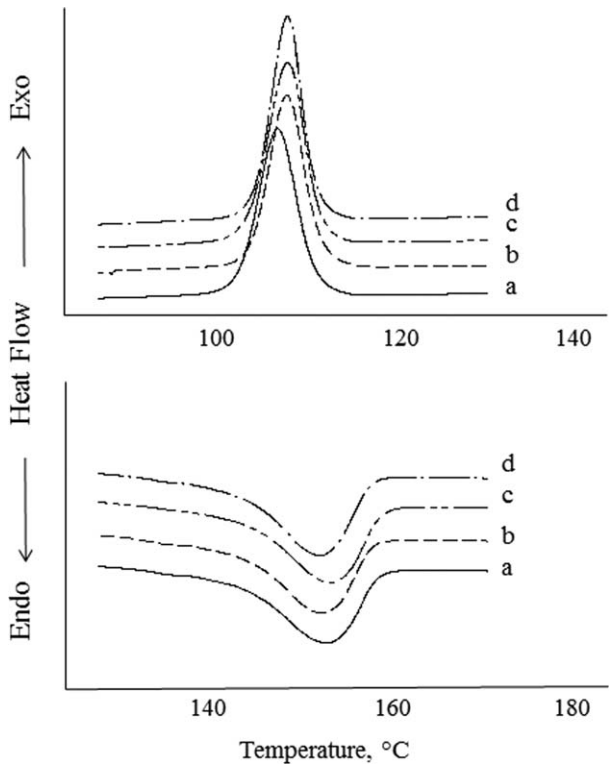

Figure 6. DSC curves of the (a) standard sample and compounds (b) 0.05% of NpAg_silica (c) 0.3% of Ag^+_phosphate, and (d) 2% of Ag^+_bentonite.

Table III. DSC Results of the Second Heating of TPE Samples

Sample	T_m (°C)	ΔH_m (J g^{-1})	T_c (°C)	ΔH_c (J g^{-1})	X_c (%)
PP	166	89	113	90.6	43
Standard	153	21	107	21.4	48
Ag^+_phosphate (0.1%)	152	21	108	21.2	48
Ag^+_phosphate (0.3%)	152	20	108	20.1	45
NpAg_silica (0.025%)	152	20	108	20.9	46
NpAg_silica (0.050%)	153	21	108	21.8	48
Ag^+_bentonite (0.5%)	153	20	108	20.8	46
Ag^+_bentonite (2.0%)	152	21	108	21.3	48

PP is strongly susceptible to additives that change its crystallization feature by accelerating crystallization.[49] In an experiment performed by Chan (2002),[50] the addition of $CaCO_3$ did not change crystallinity of PP, but the crystallization temperature increased by about 10 °C. The size of the spherulites decreased with the increase of $CaCO_3$, as it works as a nucleating agent. In sum, the particles of the additive acted as nucleation sites, reducing the spherulites size, which increase the crystallinity and, consequently, the modulus.[51,52]

In this study, the incorporation of the additives resulted in a slight difference in the crystallinity values. Whereas that to some authors the polymer crystallinity influences the additive efficiency, by promoting the silver migration to the surface of the compound[12–15] and in the case of silver nanoparticles, water must be diffused by the amorphous portion of the compound, it could be assumed that the better antibacterial activity of NpAg_silica was related to the portion of amorphous area presented in the compound.

Morphology. Figure 7 shows scanning (a,d, and g) and transmission microscopies of the compounds with 0.05% of NpAg_silica (a,b,c); 0.3% of Ag^+_phosphate (d,e,f), and 2% of Ag^+_bentonite (g,h,i). As immiscible components, blends of SEBS, PP, and oil always will form two separated phases: a SEBS/oil and PP/oil domains. In TEM images, these domains were presented as dark (SEBS/oil) and bright (PP/oil) areas.[53] The SEM images did not provide any information, because of the little size of the additives. In Figure 7(g), it was possible to see a sheet of bentonite.

In TEM analysis, in the first images for all additives was remarkable the preference of the particles to SEBS/oil phase. For NpAg_silica, it was noted that the silica particles formed agglomerates [Figure 7(b,c)]. The bentonite sheets did not exfoliate; instead of this they formed clusters [Figure 7(h,i)].

Antimicrobial Studies. Table IV shows bacterial reduction (%) and antibacterial efficacy (R) values in metal loaded TPE toward *E. coli* and *S. aureus* populations. Figure 8(a,b) show bacterial reduction of *E. coli* and *S. aureus* populations, respectively, in additived TPE monitored in a 24-h period.

E. coli ($F_{5,12} = 11.5521$; $P < 0.05$) and *S. aureus* ($F_{5,12} = 7.509$; $P < 0.05$) final population differs significantly between the antibacterial additives. All the samples eliminated more than 90% of *E. coli* CFU after 24 h. Only NpAg_silica eliminated more than 80% of *S. aureus*. This suggested differences in antimicrobial activity. None of the additives reached the value of R required by standard JIS Z 2801, even in the maximum dose recommended by the additive suppliers.

It was noted that the sample with 0.1% Ag^+_phosphate was more effective than the sample 0.3%, the same occured with sample NpAg_silica, which could be due to inefficient dispersion of the additive during processing.

It was reported that the contact of silver ions (positively charged) with the bacterial wall (negatively charged) causes an electrostatic imbalance that induces a sequence of events leading to a disturbance of bacterial cell structure, and may hinder microbial proliferation.[54,55] In addition, ionic silver can block DNA transcription and suspend bacterial respiration and adenosine triphosphate synthesis.[56] According to Kim *et al.* (2011)[57] bacterial membranes possess sulfur-containing proteins and silver nanoparticles penetrate the cell by connecting to these proteins. After entering the bacterial cell, silver nanoparticles react with the respiratory chain of bacteria and inhibit their respiration.

The biocidal activity of nanoparticles is amplified by its topography, that improves contact with the microorganisms.[58] Silver nanoparticles are a small form of elemental silver and still there is no consensus on its way of action. Martínez-Abad (2012)[59] describes silver nanoform with unstable behavior resembling an ion in action. Tolaymat *et al.* (2010)[60] mention that when silver nanoparticles come in contact with the dissolved oxygen ($O_{2(aq.)}$) in water, they release silver ions according to the following equation:

$$O_{2(aq.)} + 4H_3O+ + 4Ag_{(s)} \rightarrow + 4Ag^+{}_{(aq.)} + 6H_2O$$

E. coli was more responsive to the toxic effects of silver. This configuration may be due to the thin peptidoglycan layer found in Gram-negative cell walls that allows the permeation of silver particles into the cytoplasm. Sondi and Salopek-Sondi (2004)[61] studied the interaction between *E. coli* and silver at the nanometer scale. They found indications of deterioration similar to pits in the surface membrane of bacteria. This characteristic kills the bacteria by raising membrane permeability, which prevents an appropriate control of molecule being transported across the membrane. In addition, Morones *et al.* (2005)[62] described the bactericidal action of silver nanoparticles by association and harm to DNA, indicating a nano-size dependent relationship in biocide effect.

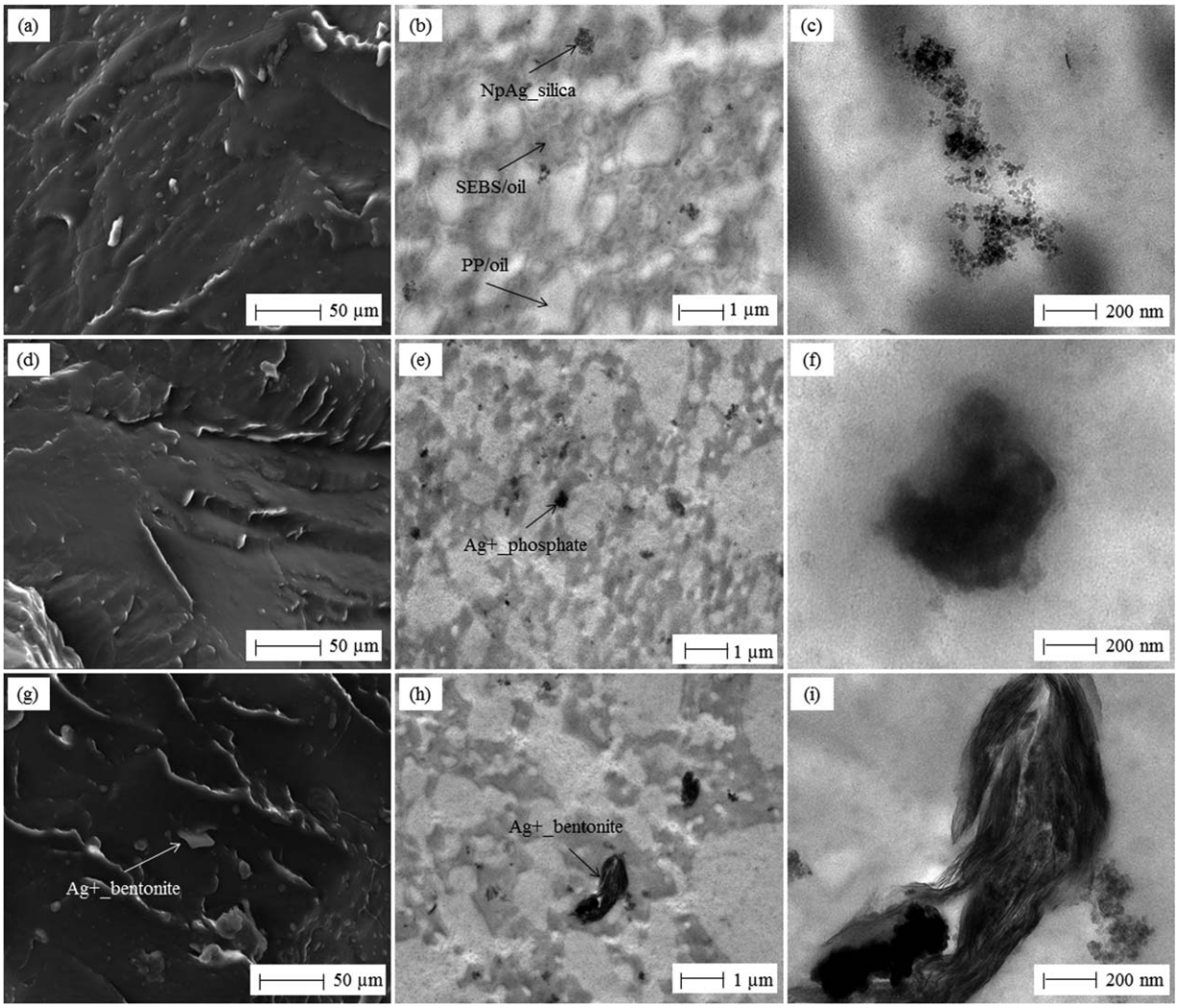

Figure 7. SEM (a,d, and g) and TEM of the compounds with 0.05% of NpAg_silica (a,b,c); 0.3% of Ag^+_phosphate (d,e,f), and 2% of Ag^+_bentonite (g,h,i).

It is noteworthy that, as in our study, previous research using silver-based additives reported a level of tolerance to silver in Gram-positive bacteria.[18,23] These results could be due the thick peptidoglycan cell wall of Gram-positive bacteria that protects its cell from silver penetration.[63] Thus, the form of incorporation of silver into different bacterial cell walls influence its efficiency, especially toward the bacterium *S. aureus*, which is known to have a higher resistance.

One aspect that remains to be established concerns the identification of exactly which of the physical and chemical properties of nano-Ag are responsible for the effective antibacterial activities of silver compounds materials.[64] As that high surface area means more contact area available,[65] the enhanced effect of NpAg_silica can be explained by the high SSA observed in these additives (45× bigger than Ag^+_phosphate and 8x bigger than Ag^+_bentonite). As describe by Magaña *et al.* (2008)[44] the antibacterial properties of silver exchanged montmorillonites have been attributed to the attraction of the negatively charged membrane of the bacteria to the surface of the clay, where silver ions kills the bacteria or renders them unable to replicate. In this study, the low SSA and overlapping sheets of the additive Ag^+_bentonite may have limited the contact of bacteria with the bentonite surfaces coated with silver.

The high crystalinnity of the compound (almost 50%) may have hindered the release of ions to the specimen surface. The additives evaluated herein have been developed and are

Table IV. Variation of Antimicrobial Efficacy

	E. coli		*S. aureus*	
	Reduction (%)	*R*	Reduction (%)	*R*
Ag^+_bentonite (0.5%)	95.3	0.5	26.8	0.6
Ag^+_bentonite (2.0%)	95.3	0.5	76.4	1.1
Ag^+_phosphate (0.1%)	95.6	0.5	57.3	0.8
Ag^+_phosphate (0.3%)	92.0	0.2	43.4	0.7
NpAg_silica (0.025%)	96.4	0.6	81.9	1.2
NpAg_silica (0.050%)	95.6	0.5	80.6	1.1

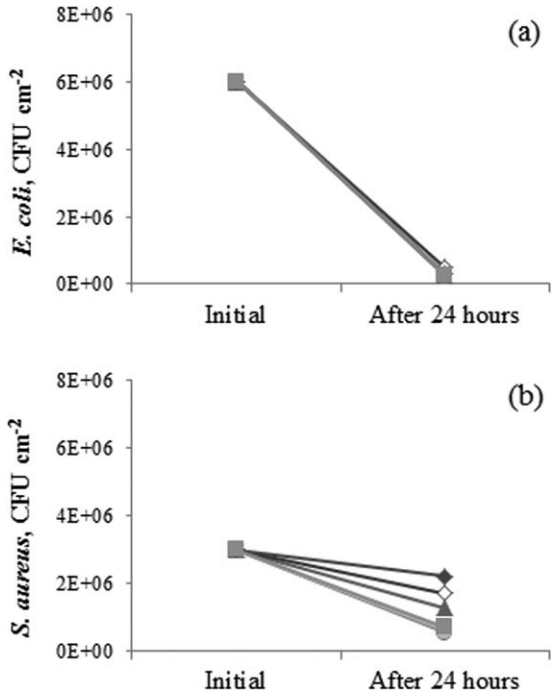

Figure 8. Variation in (a) *E. coli* and (b) *S. aureus* CFU per square centimeter (CFU cm^{-2}) in (-○-) NpAg_silica 0.025%, (-•-) NpAg_silica 0.05%, (-▲-) Ag^+_phosphate 0.1%, (-¤-) Ag^+_phosphate 0.3%, (-◆-) Ag^+_bentonite 0.5%, (-■-) Ag^+_bentonite 2.0% compounds.

recommended for use in thermoplastics such as polypropylene, polystyrene and polyethylene. However, as previously mentioned, the use of antibacterial additives in TPE in a SEBS base is a market innovation. Thus, the morphological differences between these polymeric groups can affect the release of silver in its ionic or nano form, which require a higher concentration of the additive into the compound.

CONCLUSIONS

Despite being of different composition, structure and size, the additives tested here had no significant effect in tensile strength and elongation at break properties when compared to the standard sample. From an industrial point of view, changes on modulus were not considered an excluding factor for final product utilization. The NpAg_silica additive provided better efficacy, with a decrease over 90% of *E. coli* and over 80% of *S. aureus* population, probably due to its high SSA that provides a high contact with the bacteria cell, even in small amounts. Thus, the incorporation of NpAg_silica by extrusion/injection is the process that presented promising features to be applied as a biocide in SEBS-based TPE with no relevant changes to usual industrial procedures.

The process of additives dispersion should be reviewed to prevent agglomeration of the particles and achieve the maximum antimicrobial protection guaranteed by the additives suppliers.

ACKNOWLEDGMENTS

The authors would like to thank FINEP for the financial support (03.13.0280.00) and Softer Brasil Compostos Termoplásticos LTDA for infrastructure support. A special thanks to the additives suppliers TNS Nanotecnologia Ltda. and Nanobiomatters Bacti-Block, S.L. Credit for Authorship: Daiane Tomacheski is a PhD student in Materials Engineering, contributing to concept and design of the article, performed the experiments (compounds processing, additives characterization), analyze of the data, drafting, revising and editing the paper. Michele Pittol has a PhD in Biology, contributing in performing the experiments (compounds processing, additives characterization) and to drafting and revising the paper critically. Vanda Ferreira is a PhD student in Materials Engineering with a great experience in thermoplastics industry contributing to the acquisition of the financial support for the project leading to this publication, selection and acquisition of the materials, and the critical revision of the paper. Ruth Marlene is an academic professor and has broad experience in Materials Engineering, providing interpretative contributions, critical review and approval of the final version to be published.

REFERENCES

1. Drobny, J. G. Handbook of Thermoplastic Elastomers; William Andrew Inc.: Norwich, NY, **2007**; p 406.
2. Ulger, F.; Esen, S.; Dilek, A.; Yanik, K.; Gunaydin, M.; Leblebicioglu, H. *Ann. Clin. Microb. Anti.* **2009**, *8*(7). DOI: 10.1186/1476-0711-8-7.
3. Singh, S. K.; Anamika, J.; Dipak, S.; Arti, D. *Der Chem. Sin.* **2011**, *2*, 111.
4. Nandekar, K. A.; Dontulwar, J. R.; Gurnule, W. B. J. *Chem. Pharm. Res.* **2012**, *4*, 3628.
5. Gray, J. E.; Nortona, P. R.; Alnouno, R.; Marolda, C. L.; Valvano, M. A.; Griffiths, K. *Biomaterials* **2003**, *24*, 2759.
6. Temiz, A.; Toğay, S. O.; Sener, A.; Güvem, G.; Rzaev, Z. M. O.; Piskin, E. *J. Appl. Polym. Sci.* **2006**, *102*, 5841.
7. Ahmed, N. A. A. M. In Antimicrobial Polymers; Lagarón, J. M.; Ocio, M. J.; López-Rubio, A., Eds.; Wiley: Hoboken, **2012**; Vol. *1*, Chapter 2, p 23.
8. Radheshkumar, C.; Münstedt, H. *Mater. Lett.* **2005**, *59*, 1949.
9. Oliani, W. L.; Parra, D. F.; Lima, L. F. C. P.; Lincopan, N.; Lugao, A. B. *J. Appl. Polym. Sci.* **2015**, *132*, DOI: 10.1002/app.42218.
10. Sánchez-Valdes, S.; Ortega-Ortiz, H.; Ramos-de Valle, L. F.; Medellín-Rodríguez, F. J.; Guedea-Miranda, R. *J. Appl. Polym. Sci.* **2009**, *111*, 953.
11. Jokar, M.; Rahman, R. A.; Ibrahim, N. A.; Abdullah, L. C.; Tan, C. P. *Food Bioprocess Technol.* **2012**, *5*, 719.
12. Kumar, R.; Münstedt, H. *Biomaterials.* **2005**, *26*, 2081.
13. Pongnop, W.; Sombatsompop, K.; Kositchaiyong, A.; Sombatsompop, N. *J. Appl. Polym. Sci.* **2011**, *122*, 3456.
14. Palomba, M.; Carotenuto, G.; Cristino, L.; Di Grazia, M. A.; Nicolais, F.; Nicola, S. D. *J. Nanomater.* **2012**, DOI: 10.1155/2012/185029.
15. Triebel, C.; Vasylyev, S.; Damm, C.; Stara, H.; Ozpınar, C.; Hausmann, S.; Peukert, W.; Munstedt, H. *J. Mater. Chem.* **2011**, *21*, 4377.

16. Nichols, D. In Biocides in Plastics; Nichols, D., Ed.; Rapra Review Reports: United Kingdom, **2004**; Vol. *15*, Chapter 5, p 19.
17. Muñoz-Bonilla, A.; Fernandez-Garcia, M. *Prog. Polym. Sci.* **2012**, *37*, 281.
18. Jung, W. K.; Koo, H. C.; Kim, K. W.; Shin, S.; Kim, S. H.; Park, Y. H. *Appl. Environ. Microbiol.* **2008**, *74*, 2171.
19. Nawaz, H. R.; Solangi, B. A.; Zehra, B.; Nadeem, U. *Can. J. Sci. Ind. Res.* **2011**, *2*, 164.
20. Silver, S. *FEMS Microbiol. Rev.* **2003**, *27*, 341.
21. Lalueza, P.; Monzón, M.; Arruebo, M.; Santamaría, J. *Mater. Res. Bull.* **2011**, *46*, 2070.
22. Rangari, V. K.; Mohammad, G. M.; Jeelani, S.; Hundley, A.; Vig, K.; Singh, S. R.; Pillai, S. *Nanotechnology.* **2010**, *21*, 1.
23. Egger, S.; Lehmann, R. P.; Height, M. J.; Loessner, M. J.; Schuppler, M. *Appl. Environ. Microbiol.* **2009**, *75*, 2973.
24. Takamiya, A. S. Adição de Nanopartículas de Prata ao Poli (metil metacrilato) – Análise Microbiológica; Master Thesis, Universidade Estadual Paulista Júlio de Mesquita Filho, São Paulo, SP, **2010**.
25. Ferreira, L.; Fonseca, A. M.; Botelho, G.; Almeida- Aguiar, C.; Neves, I. C. *Microporous Mesoporous Mater.* **2012**, *160*, 126.
26. Kong, H.; Jang, J. *Langmuir.* **2008**, *24*, 2051.
27. Pinto, R. J. B.; Marques, P. A. A. P.; Neto, C. P.; Trindade, T.; Daina, S.; Sadocco, P. *Acta Biomater.* **2009**, *5*, 2279.
28. Jeong, S. H.; Yeo, S. Y.; Yi, S. Y. *J. Mater. Sci.* **2005**, *40*, 5407.
29. Choi, O.; Deng, K. K.; Kim, N.-J.; Ross, L. J.; Surampalli, R. Y.; Hu, Z. *Water Res.* **2008**, *42*, 3066.
30. Kumar, A.; Vemula, P. K.; Ajayan, P. M.; John, G. *Nat. Mater.* **2008**, *7*, 236.
31. Sauvet, G.; Dupond, S.; Kazmierski, K.; Chojnowski, J. *J. Appl. Polym. Sci.* **2000**, *75*, 1005.
32. Karakaya, N.; Ersoy, O. G.; Oral, M. A.; Gonul, T.; Deniz, V. *Polym. Eng. Sci.* **2010**, DOI: 10.1002/pen.21569.
33. Machado, L. D. B.; Matos, J. R. In Técnicas de Caracterização de Polímeros; Canevarolo S. V. Jr., Ed.; Artliber: São Paulo, SP, **2007**; Vol. *1*, Chapter 12, p 229.
34. JIS Z 2801, Japanese Industrial Standard; Antibacterial Products-Test for Antibacterial Activity and Efficacy; Japanese Standards Association: Tokyo, Japan, **2010**.
35. Caglar, B.; Afsin, B.; Tabak, A.; Eren, E. *Chem. Eng. J.* **2009**, *149*, 242.
36. Tian, L.; Oulian, L.; Zhiyuan, L.; Liuimei, H.; Xiaosheng, W. *Appl. Surf. Sci.* **2014**, *305*, 386.
37. Suenaga, Y.; Konaka, H.; Sugimoto, T.; Kuroda-Sowa, T.; Maekawa, M.; Munakata, M. *Inorg. Chem. Commun.* **2003**, *6*, 389.
38. Kamena, K. In Functional Fillers for Plastics; Xanthos, M., Ed.; Wiley: Weinheim, **2010**; Vol. *2*, Chapter 9, p 177.
39. Ono, H.; Ikarashi, T.; Ogura, A. *Appl. Phys. Lett.* **1998**, *72*, 2853.
40. Donchev, V.; Nesheva, D.; Todorova, D.; Germanova, K.; Valcheva, E. *Thin Solid. Films.* **2012**, *520*, 2085.
41. Lacona, F.; Franzò, G.; Spinella, C. *J. Appl. Phys.* **2000**, *87*, 1295. DOI: 10.1063/1.372013.
42. Toloman, D.; Magdas, D. A.; Bratu, I.; Giurgiu, L. M.; Ardelean, I. *Int. J. Mod. Phys. B* **2010**, *24*, 351.
43. Essehli, R.; Bali, B. E.; Benmokhtar, S.; Fuess, H.; Svoboda, I.; Obbade, S. *J. Alloy. Compd.* **2010**, *493*, 654.
44. Magaña, S. M.; Quintana, P.; Aguilar, D. H.; Toledo, J. A.; Ángeles-Chávez, C.; Cortés, M. A.; León, L.; Freile-Pelegrín, Y.; López, T.; Sánchez, R. M. T. *J. Mol. Catal. A: Chem.* **2008**, *281*, 192.
45. Orlov, A. S.; Kiselev, S. A.; Kiseleva, E. A.; Budeeva, A. V.; Mashukov, V. I. *Appl. Spectrosc.* **2013**, *80*, 47.
46. Lin, J.-H.; Pan, Y.-J.; Liu, C.-F.; Huang, C.-L.; Hsieh, C.-T.; Chen, C.-K.; Lin, Z.-I.; Lou, C.-W. *Materials.* **2015**, *8*, 8850.
47. Wu, C. L.; Zhang, M. Q.; Rong, M. Z.; Friedrich, K. *Compos. Sci. Technol.* **2005**, *65*, 635.
48. Xanthos, M. In Functional Fillers for Plastics; Xanthos, M., Ed.; Wiley: Weinheim, **2010**; Vol. *2*, Chapter 2, p 19.
49. Stribeck, N.; Zeinolebadi, A.; Sari, M. G.; Botta, S.; Jankova, K.; Hvilsted, S.; Drozdov, A.; Klitkou, R.; Potarniche, C.-G.; Christiansen, J. D.; Ermini, V. *Macromolecules.* **2012**, *45*, 962.
50. Chan, C.-M.; Wu, J.; Li, J.-X.; Cheung, Y.-K. *Polym. J.* **2002**, *43*, 2981.
51. Way, J. L.; Atkinson, J. R.; Nutting, J. *J. Mater. Sci.* **1974**, *9*, 293.
52. Parenteau, T.; Ausias, G.; Grohens, Y.; Pilvin, P. *Polymer.* **2012**, *53*, 5873.
53. Segupta, P. Morphology of Olefinic Thermoplastic Elastomer Blends; PhD. Thesis, University of Twente, Enschede, The Netherlands, **2004**.
54. Hamouda, T.; Baker, J. R. Jr. *J. Appl. Microbiol.* **2000**, *89*, 397.
55. Stoimenov, P. K.; Klinger, R. L.; Marchin, G. L.; Klabunde, K. J. *Langmuir.* **2002**, *18*, 6679.
56. Trevors, J. T. *Enzyme. Microb. Technol.* **1987**, *9*, 331.
57. Kim, S. S.; Park, J. E.; Lee, J. *J. Appl. Polym. Sci.* **2011**, *119*, 2261.
58. Raghupathi, K. R.; Koodali, R. T.; Manna, A. C. *Langmuir.* **2011**, *27*, 4020.
59. Martínez-Abad, A. In Antimicrobial Polymers; Lagarón, J. M.; Ocio, M. J.; López-Rubio, A. Eds.; Wiley: Hoboken, **2012**; Vol. *1*, Chapter 11, p 287.
60. Tolaymat, T. M.; Badawy, A. M. E.; Genaidy, A.; Scheckel, K. G.; Luxton, T. P.; Suidan, M. *Sci. Total Environ.* **2010**, *408*, 999.
61. Sondi, I.; Salopek-Sondi, B. *J. Colloid Interface Sci.* **2004**, *275*, 177.
62. Morones, J. R.; Elechiguerra, J. L.; Camacho, A.; Holt, K.; Kouri, J. B.; Ramírez, J. T.; Yacaman, M. *J. Nanotechnol.* **2005**, *16*, 2346.
63. Fortunati, E.; Armentano, I.; Zhou, Q.; Iannoni, A.; Saino, E.; Visai, L.; Berglund, L. A.; Kenny, J. M. *Carbohydr. Polym.* **2012**, *87*, 1596.
64. Lok, C.-N.; Ho, C.-M.; Chen, R.; He, Q.-Y.; Yu, W.-Y.; Sun, H.; Tam, P. K.-H.; Chiu, J.-F.; Che, C.-M. *J. Biol. Inorg. Chem.* **2007**, *12*, 527.
65. Ciullo, P. A. Industrial Minerals and Their Uses: A Handbook and Formulary; Noyes Publication: Westwood, **1996**; p 640.